ACS APPLIED MATERIALS & INTERFACES

Research Article

www.acsami.org

Hollow, Spherical Nitrogen-Rich Porous Carbon Shells Obtained from a Porous Organic Framework for the Supercapacitor

Xianhu Liu, Lei Zhou, Yongqing Zhao, Lei Bian, Xiaotong Feng, and Qiaosheng Pu*

State Key Laboratory of Applied Organic Chemistry, Key Laboratory of Nonferrous Metal Chemistry and Resources Utilization of Gansu Province, College of Chemistry and Chemical Engineering, Lanzhou University, Lanzhou 730000, China

Supporting Information

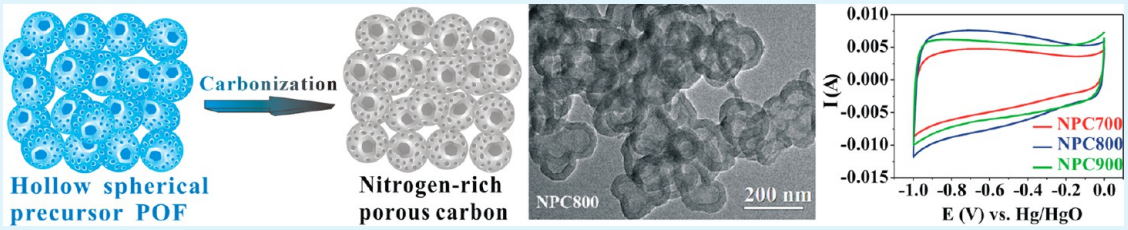

ABSTRACT: Hollow, spherical nitrogen-rich porous carbon shells were prepared as supercapacitor electrode materials through the carbonization of structure-controlled porous organic frameworks at high temperature. The structure and electrochemical properties of the resulting carbonized materials were systematically characterized. Experimental results revealed that the nitrogen-rich hollow carbon spheres obtained at 800 °C were a kind of amorphous carbon with micropores on the shell frame and with specific surface areas as high as 525 $m^2 g^{-1}$. The prepared porous carbon possessed a specific capacitance of 230 F g^{-1} at a current density of 0.5 A g^{-1} and could retain ~98% of the initial capacitance after 1500 successive charge−discharge cycles. Electrochemical impedance spectroscopy indicated that the material has a small equivalent series resistance (0.62 Ω). All of these values demonstrated that the prepared porous carbon is a promising supercapacitor material. The proposed method represents a simple approach towards the preparation of unique structures of nitrogen-containing porous carbon that exhibit the advantages of having a simple preparation process, a wide availability of precursors, flexible control of the structure, and an easier adjustment of the amount of heteroatoms.

KEYWORDS: *porous organic framework, carbonization, nitrogen-rich porous carbon, supercapacitor, hollow sphere*

1. INTRODUCTION

Because of the advantages of rapid charge−discharge,[1,2] high-energy (power) density,[3,4] good recyclability,[5] small size, and environmental safety,[6] supercapacitors have been widely used in the fields of electric vehicles, portable electronic equipment, and emergency power supplies.[7] In recent years, many investigators have been devoted to comprehensive and intensive studies on supercapacitors to improve their performance. The electrode material,[8−12] as an important factor affecting the properties of a supercapacitor, has remained a hot spot of the research in this direction.

The carbon-based supercapacitor electrode materials, such as activated carbon,[13] carbon nanotube,[14] and graphene,[15] store energy via an electric double-layer mechanism.[16] The supercapacitor with these materials exhibits good electrochemical stability, but their capacitance could hardly obtain a great breakthrough because of the limitations arising from their structure. Recently, investigators found that the capacitance of carbon-based supercapacitors could be improved through internal or surface doping of heteroatoms (N and O).[17] It has been shown that the heteroatoms could store energy through pseudocapacitance, which is based on a Faradaic reaction mechanism. Denisa et al.[18] systematically investigated the effect of heteroatoms on the capacitive properties of microporous activated carbon. Carbonization of nitrogen-containing precursors[19−21] and postmodification[22] were frequently employed in these works to introduce heteroatoms to carbon-electrode materials. However, these methods suffer from problems such as the lack of effective control of the pore sizes or structures and the tedious procedure for the postmodification. Exploring novel ways to solve these problems are among the most important tasks for improving the performance of carbon-based supercapacitors.

In the past few years, porous inorganic and organic materials have been successfully used in catalysis,[23,24] sensors,[25,26] gas storage or separation,[27,28] and adsorption.[29,30] On the basis of the different design strategies, these include porous organic frameworks (POFs), which are also referred to as hypercrosslinked polymers (HCPs),[31,32] polymers of intrinsic microporosity (PIMs),[33,34] conjugated microporous polymers (CMPs),[35,36] and covalent organic frameworks (COFs).[37] POFs possess superior thermal and chemical stability. By proper selection of the precursors and synthetic methods, POFs can be prepared with different pore sizes and structures. In

Received: August 1, 2013
Accepted: September 20, 2013
Published: September 20, 2013

addition, various functional groups can also be introduced onto the surface of the pores. These unique characteristics offer POFs great potential for use in practical applications. Lately, researchers have attempted the application of POFs in electrochemistry. Ding et al.[38] has synthesized an n-channel 2D COF (2D-NiPc-BTDACOF) with an excellent electron-transfer rate (0.6 cm^2 V s^{-1}), which behaves over the full spectrum of the photoelectric effect and is susceptible to the near-infrared range. Kou et al.[39] synthesized an Aza-fused p-conjugated microporous framework via an ion thermal method. The polymer organic materials exhibit outstanding capacitive properties, with a capacitance of 946 F g^{-1} at a current density of 0.1 A g^{-1} and a maximum energy density and power density of 53 W h kg^{-1} and 2.25 kW kg^{-1}, respectively. However, the electrical conductivity of most POFs is unsatisfactory, which limits their use in electrochemistry. Therefore, efforts should be made to improve the electrical conductivity of POFs.

Feng et al.[40] synthesized conjugated polymer networks of polyphenylene (CPNs) via a Hagihara–Sonogashira coupling reaction using 1,3,5-tris-2′-biphenylbenzene as a starting material, which were used as precursors to obtain carbon materials (Py-CPNs). The CPNs and Py-CPNs possessed a morphology of a 1D carbon nanotube or carbon nanofiber. The largest specific area and highest specific capacitance were 900 m^2 g^{-1} and 115 F g^{-1} (1 mV s^{-1}), respectively. Liang et al.[41] synthesized alkyl-substituted hyperbranched polyphenylene via anodic alumina membranes as the template, and the polyphenylene was used to obtain 1D mesoporous carbon (MPNC). The specific area of these MPNCs could reach 1140 m^2 g^{-1}, and their pore diameters were distributed over a range of 10–20 nm. When these MPNCs were used as the electrode materials of supercapacitors, their specific capacitance reached 304 F g^{-1} at a scanning rate of 5 mV s^{-1}. Recently, carbonization with porous Schiff-base networks (SNWs) of melamine and terephthalaldehyde for the porous carbon was reported,[42] and a specific capacitances of 381 F g^{-1} under acidic conditions and 351 F g^{-1} under alkaline conditions were achieved. All of these works indicate that carbonization of POFs is an effective way to produce unique carbon materials. Meanwhile, because the structure of POFs could be tailored through either the synthesis procedure or extra additives, it renders huge possibilities for the morphology of the resulting carbon, which may play an important role in the performance of capacitive materials.

In the present study, hollow, spherical nitrogen-rich porous carbon shells were obtained through carbonization of a POF (Figure 1), and its feasibility for use as the electrode material of a supercapacitor was investigated. The excellent controllability of the pore size, structure, and functional groups of POFs greatly facilitates the formation of the nitrogen-containing porous carbon shells that may be competent for supercapacitors. The hollow-shell-like porous structure together with further modification of the pore size and nitrogen content through carbonization added more flexibility for the performance manipulation.

Figure 1. Schematic illustration of the synthesis of nitrogen-rich porous carbon.

2. EXPERIMENTAL SECTION

2.1. Synthesis. The precursor POF was synthesized according to a previously published protocol with a slight simplification.[24] Briefly, 48 mg of 1,3,5-triformylbenzene and 48 mg of *p*-phenylenediamine were dissolved in 3 mL of 1,4-dioxane. The mixture was then transferred into a 20 mL glass ampule. After adding 0.6 mL of 3M aqueous acetic acid, the mixture was flash frozen using a liquid-nitrogen bath. The ampule was sealed with the aid of an alcohol blast burner after degassing for 5 min. When warming to room temperature, the glass ampule was placed vertically in an ampule holder and heated in an oven at 120 °C for 3 days. The reaction product was vacuum filtered and washed with DMF (30 mL × 3), THF (30 mL × 3), and dichloromethane (30 mL × 3) successively. The obtained product was dried under vacuum at 60 °C for 24 h and kept in a desiccator before the carbonization. The yield was calculated to be 85%.

The prepared POF (100 mg per batch in a ceramic boat) was carbonized at different temperatures under a nitrogen atmosphere (constant flow at 112 mL min^{-1}) in a tube furnace. The temperature was first heated to 200 °C at an increasing rate of 15 °C min^{-1} and was held at this temperature for 1 h. The temperature was then raised to a predetermined value at a rate of 12 °C min^{-1} and was maintained at that temperature for 3 h.

2.2. Characterization. Scanning electron microscopic (SEM) images were obtained from a JSM-6701F field-emission scanning electron microscope with an accelerating voltage of 5 kV. Finely ground sample was dispersed into ethanol with the aid of an ultrasonic bath and dropped on a flat copper sample holder to dry. The sample was then coated with a gold film to facilitate conduction using an E-1045 sputter coater. A JEOL JEM-2010 transmission electron microscope (TEM) operated at 200 kV was used to observe the size and morphology of the materials. X-ray diffraction (XRD) data were obtained from a PANalytical X′Pert Pro X-ray diffractometer at 40 kV and 40 mA with Cu Kα radiation (λ = 1.54056 Å). Infrared spectra were recorded on a Thermo Nicolet NEXUS 670 Fourier-transform infrared spectrometer using KBr pellets. Elemental analyses were conducted on a Vario EL elemental analyzer (Elementar, Germany). The nitrogen adsorption and desorption isotherms were measured at 77 K using a Micromeritics ASAP 2020M system. The samples were outgassed at 120 °C for 3 h before the measurements. The specific surface areas for N_2 were calculated using the Brunauer–Emmet–Teller (BET) model. The pore size distributions were calculated from the adsorption isotherms by the original density functional theory model. Powder XPS data were collected from a VG (ESCALAB210) multifunctional X-ray photoelectron spectrometer. Raman spectra were recorded on a Nicolet Raman 950 Fourier-transform Raman spectrometer.

2.3. Electrochemical Analysis. All of the electrochemical experiments were conducted on a CHI660D electrochemical workstation. The working electrode was prepared according to the following steps: the carbonized product (85 wt %), acetylene black (10 wt %), and polytetrafluoroethylene (5 wt %) were mixed sufficiently, and the mixture was pressed to a sheet with nickel net (1 cm^2). The electrochemical properties of the electrode were measured by cyclic voltammetry (CV), galvanostatic charge–discharge (GCD), and electrochemical impedance spectroscopy (EIS). KOH (5 mol L^{-1}) was used as the electrolyte solution, platinum foil was used as the counter electrode, and Hg/HgO was used as the reference electrode. The capacitance was calculated on the basis of the galvanostatic charge and discharge curve according to the following equation

$$C_s = \frac{I\Delta t}{m\Delta V}$$

where C_s (F g^{-1}) is the specific capacitance, I (A) is the discharging current, Δt (s) is the discharging time, m (g) is the amount of the sample used for the preparation of the electrode, and ΔV (V) is the change of voltage during the discharging process.

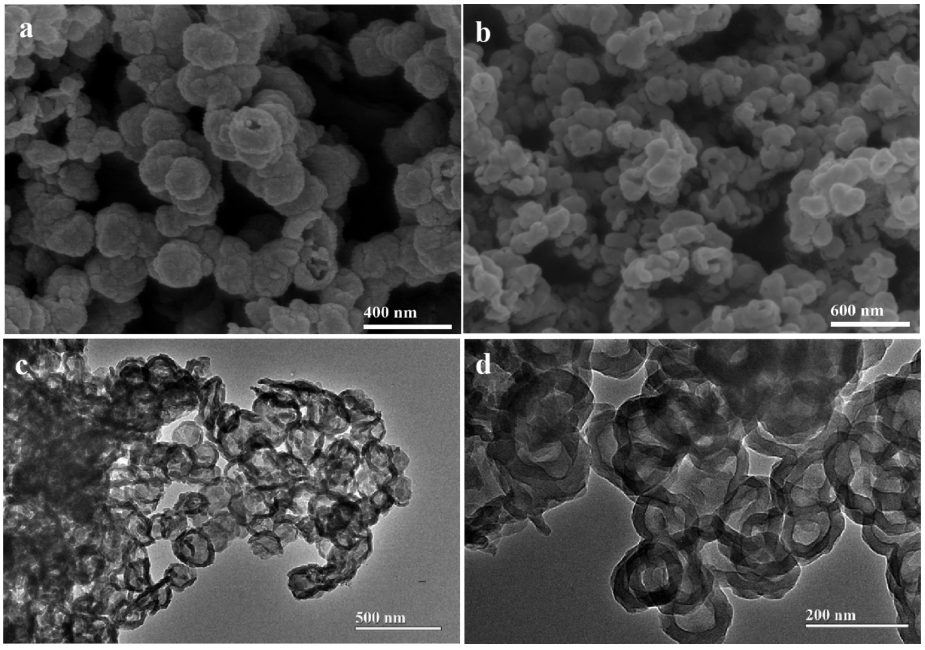

Figure 2. SEM images of (a) the precursor POF and (b) NPC800 and TEM images of (c) the precursor POF and (d) NPC800.

3. RESULTS AND DISCUSSION

3.1. Characterization. The SEM photographs (Figure 2a) indicated that the precursor POF was mainly composed of hollow spheres. The cavity inside the precursor POF sphere might be formed because of trapped solvent during the polymerization. The diameters of these spheres were in a range from 150 to 250 nm. However, the diameter of the product particles carbonized at 800 °C (referred to as NPC800) was about 130 nm (Figure 2b), which is smaller than the precursor. The carbonized products exhibited roughly the same morphology as the precursor except for some shrinkage, which was a reasonable consequence of the loss of H and the structural change after carbonization. The diameters of the spheres measured from the TEM images before and after carbonization were 176 ± 19 and 144 ± 17 nm, respectively. The shells experienced the same shrinkage, which was 29 ± 7 nm for the precursor POF and 24 ± 5 nm for NPC800 (Figure 2c,d). The sizes measured from the SEM images were a little bigger (228 and 178 nm, respectively), possibly because of gold sputtered on the materials. The XRD pattern (Figure S2) showed that NPC800 was amorphous.

The nitrogen content of the carbonized materials obtained at different temperatures are given in Table 1. It was found that the highest nitrogen content was obtained at 700 °C. A decrease of nitrogen content at 900 °C might be a consequence of the breakage of the N−C bond because it might decompose quickly at temperatures over 850 °C.[43] The XPS (Figure 3a) results showed the surface elements of the precursor and carbonized POFs. The carbonized materials were composed of C, O, and N, which is in agreement with the results of the element analysis. Additionally, XPS (Figure 3, panels b and f) results indicated that there was only one kind of N on the surface of the precursor POF, which was the Schiff base nitrogen (N−S),[44] based on the structure of the precursor and the binding energy value of 399.1 eV. Two types of N were found on the surface of the carbonized materials (Figure 3, panels b and c−e). The characteristic peaks were 398.8 and 400.8 eV, which could be attributed to pyridinic (N-6) and quaternary (N-Q) nitrogen,[22] respectively. Moreover, the ratios of N-Q and N-6 for NPC700, NPC800, and NPC900 were 0.77, 1.45, and 2.48, respectively, suggesting a better stability of N-Q than that of N-6 at a higher temperature.

Table 1. Pore Properties and Nitrogen Content of the Precursor POF and Carbonized Products

sample name	S_{BET} (m^2 g^{-1})[a]	d_{pore} (nm)[b]	V_{total} (cm^3 g^{-1})[c]	N (%)[d]
precursor POF	398	4.8	0.48	14.34
NPC700	357	4.9	0.43	12.89
NPC800	525	5.2	0.67	4.73
NPC900	398	4.9	0.48	2.21

[a]BET surface area. [b]Adsorption average pore width (4 V/A by BET). [c]Single-point adsorption total pore volume of pores at P/P_0 = 0.988. [d]Nitrogen content.

FTIR (Figure 4a) was used to determine the functional groups of the precursor POF and the carbonized materials. The precursor showed absorption peaks at 1621, 3437, and 1698 cm^{-1}, which could be assigned to the imine bond (C═N) as well as the unreacted amino (NH_2) and aldehyde (HC═O) groups. These three characteristic peaks were also present in the FTIR spectra of the carbonized materials, but they varied from sharp and strong peaks for the precursor to broad and weak bands for the carbonized products as a result of the reduction and decomposition of the functional groups. Bands at 3437 and 1621 cm^{-1} can be attributed to the incompletely carbonized NH_2 and C═N, respectively, whereas the band at 1244 cm^{-1} may correspond to the C−N bond. In addition, we find that the intensity of the C═N bond decreased, whereas that of C−N increased with the elevated temperature, indicating that the C═N bond reduced to a C−N bond at the high temperature. There are two broad characteristic peaks (1357 and 1578 cm^{-1}) in the Raman spectra (Figure 4b) of the carbonized materials, which correspond to the D band, caused by the defects in the graphene structure, and the G band, caused by in-plane vibrations of the graphitic structure.[45] The

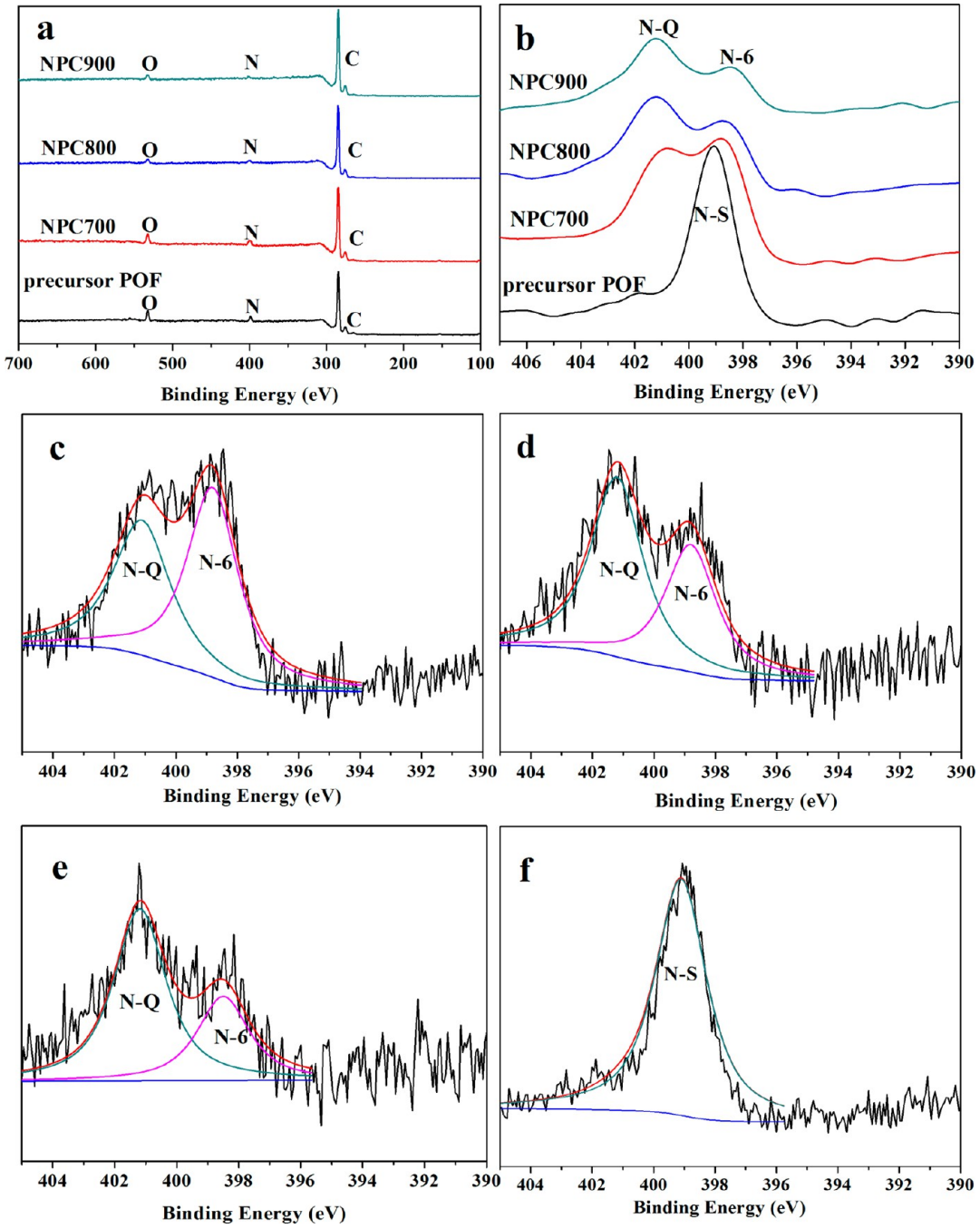

Figure 3. (a) XPS survey spectra of the precursor POF, NPC700, NPC800, and NPC900. (b–f) High-resolution XPS spectra of the deconvoluted N 1s peak: (c) NPC700, (d) NPC800, (e) NPC900, and (f) precursor POF.

intensity ratio of the D and G bands (I_D/I_G) suggests the graphitization of the carbon materials, a lower I_D/I_G value, less defects, and sp^3 carbon atoms, which means a higher degree of graphitization. The I_D/I_G values for NPC700, NPC800, and NPC900 were 1.07, 0.98, and 0.98, respectively, which implied a higher degree of graphitization when the temperature increased from 700 to 800 °C, but further elevation of temperature could not eliminate more defects.

Nitrogen adsorption and desorption experiments (Figures 5, S3a, and S4a) showed type II adsorptive curves and H3 desorptive curves both for the precursor POF and the carbonized material, which demonstrated the existence of both micro- and mesopores in these materials. It should be mentioned that the shells themselves are porous because of the rigid structure of the monomers, just like that in other POFs, which was also verified by the pore size distribution (inset of Figure 5). Additionally, the specific surface area changed with the carbonization temperature, and the product carbonized at 800 °C (NPC800) possessed the highest specific surface area, 525 $m^2\ g^{-1}$. The increase of the specific surface area when increasing the carbonization temperature from 700 to 800 °C might result from the increase of the extent of the carbonization, whereas the decrease of the surface area at 900 °C might relate to the decomposition of the C–N structure and the collapse of the pore structure that it caused. This presumption was supported by the pore size distribution (inset

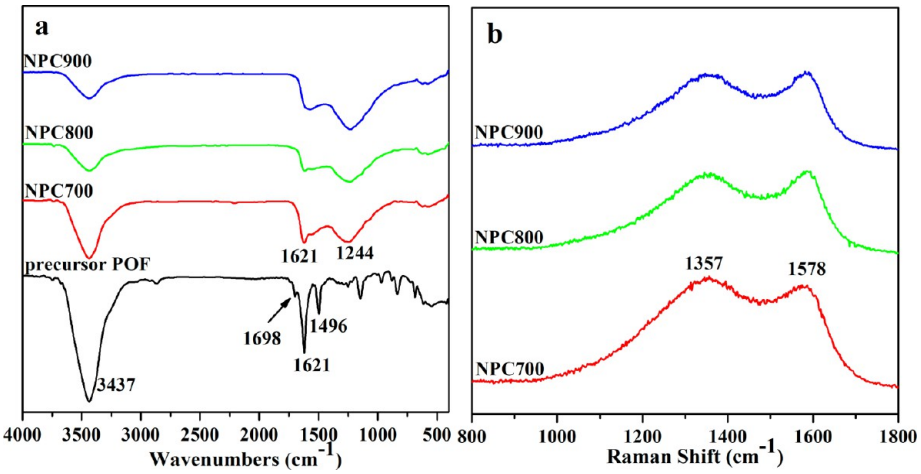

Figure 4. (a) FTIR spectra of the precursor POF, NPC700, NPC800, and NPC900. (b) Raman spectra of NPC700, NPC800, and NPC900.

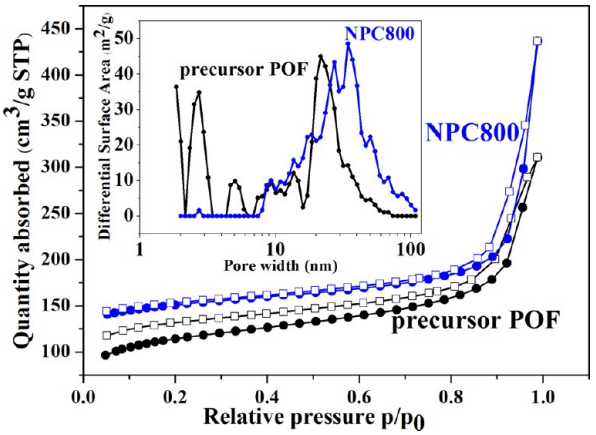

Figure 5. Nitrogen adsorption−desorption isotherms of the precursor POF and NPC800 (the inset shows the pore size distribution).

of Figures 5, S3b, and S4b) of the materials carbonized at various temperatures. It was apparent that the number of microporous pore decreased, whereas the number of meso- and macroporous pore increased with the increase of the carbonization temperature. The pore size distribution of NPC800 indicated that there were micropores, mesopores, and a small amount of macropores. This kind of pore distribution, especially the presence of the hollow structure, was beneficial to the improvement of the capacitive properties, as will be discussed in detail in the following section.

3.2. Electrochemical Analysis. The CV curves of the precursor POF (Figure S1) showed a pair of symmetric redox peaks, which indicated that the precursor POF could not be directly used as the supercapacitor material. Its poor conductivity was another obstacle for its use as the electrode material. To improve its conductivity and to obtain a more porous structure, the precursor POF was carbonized at a high temperature under an atmosphere of N_2. (The effect of carbonization on the structure has been discussed above.) To check their applicability as supercapacitor electrode materials, the capacitive properties of the products carbonized at the different temperatures (700, 800, and 900 °C) were systematically investigated. The cyclic voltammetry experiments (Figure 6a) indicated that NPC800 possessed the highest specific capacitance.

CV, GCD, and EIS were used to investigate the electrochemical properties of the produced materials in the three-electrode format using 5 mol L^{-1} KOH as the electrolyte. Figure 6a shows that the materials carbonized at all three temperatures displayed quasi-rectangular CV curves at a scanning rate of 5 mV s^{-1}, which implies the superior capacitive properties of these materials. Because of its large surface area as

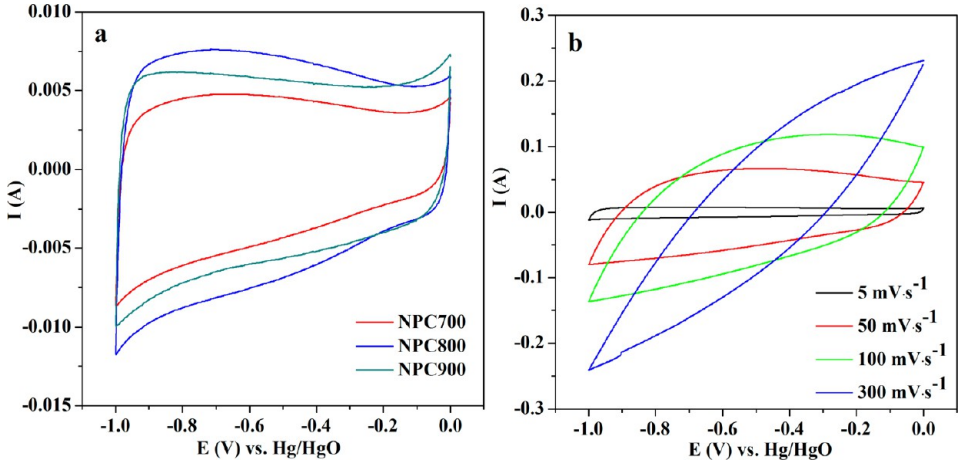

Figure 6. (a) CV curves of NPC700, NPC800, and NPC900. (b) CV curves of NPC800 at scan rates of 5, 50, 100, and 300 mV s^{-1}.

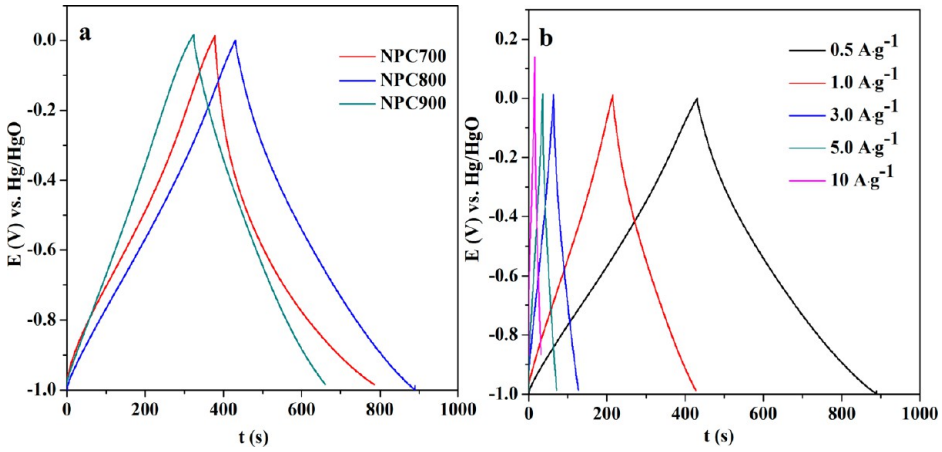

Figure 7. (a) GCD cycling of NPC700, NPC800, and NPC900 at a current density of 0.5 A g^{-1}. (b) GCD cycling of NPC800 at current densities of 0.5, 1, 3, 5, and 10 A g^{-1}.

well as the proper pore size distribution, NPC800 gave the largest quasi-rectangular area, namely, the highest specific capacitance. Figure 6b illustrates the CV curves of NPC800 at different scanning rates. It is evident that NPC800 retained a quasi-rectangular CV response at a scanning rate as high as 100 mV s^{-1}, indicating the fast electron transfer and electrolyte transportation.

GCD curves of the carbonized materials were all triangular (Figure 7a), which confirmed their excellent performance as supercapacitors. It is worth mentioning that owing to the presence of nitrogen in the materials, part of the triangle edges deviate from the straight line. Additionally, their very low voltage drop indicated the small internal resistance inside the materials. The specific capacitance of the materials could be calculated according to the discharging time of the GCD. NPC800 showed the longest discharging time and possessed the highest specific capacitance, 230 F g^{-1} was calculated at a current density of 0.5 A g^{-1}, which was in agreement with the conclusion obtained from the CV experiments. The highest specific capacitance might come from the highest specific surface area and adequate pore size distribution of NPC800, which was beneficial to the formation of an electric double layer. In addition, nitrogen in the carbon structure might undergo a reversible redox reaction, which would contribute to the pseudocapacitance. More importantly, the introduction of nitrogen could improve the surface wettability. Together with the hollow structure, the better wettability was favorable to the permeation of electrolyte solution into the pores of the materials, and the large specific surface area could be utilized more efficiently. There was no obvious redox peak in the CV curves, indicating that the electric double layer was the main source of the capacitance. Figure 7b illustrates the GCD curves of NPC800 at different current densities. It can be seen that the GCD curves of NPC800 appear as symmetric triangles even at a current density as high as 10 A g^{-1}.

The supercapacitive properties of the materials could be also characterized via EIS. Figure 8 is the Nyquist plots of the material obtained at different temperatures. The EIS curve of NPC800 was much closer to the *y* axis, indicating that NPC800 behaved as a more ideal supercapacitor. The high-frequency region (inset of Figure 8) showed that the curve of NPC800 possessed the smallest semicircular radius, indicating the minimum equivalent series resistance (ESR) (0.62 Ω).[46] This indicated that the ion diffusion and electrolyte permeation into

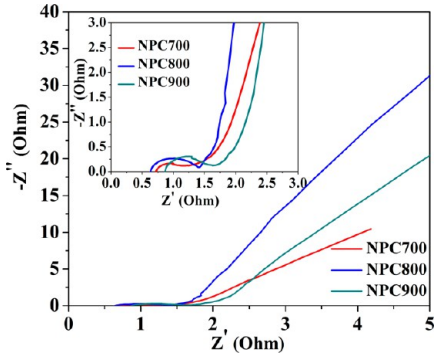

Figure 8. EIS spectra of NPC700, NPC800, and NPC900 (the inset shows the magnified view of the initial range).

the pore channels was easier, which might facilitate the formation of the electric double layer. In addition, the lower ESR of NPC800 might also relate to the lower nitrogen content confirmed by the elemental analysis because the ESR value might be a result of the reversible redox reaction of nitrogen.[47] Of course, the larger ESR values of NPC700 and NPC900 might be also caused by their lower specific surface areas and smaller pore sizes, which hindered the ion diffusion and electrolyte penetration.

The change of the specific capacitance of the carbonized materials at different current density is shown in Figure 9. NPC800 had the highest specific capacitance at all tested current densities, 230 and 190 F g^{-1} were obtained at current densities of 0.5 and 3 A g^{-1}, respectively, reflecting a better capacitance-retention capability of these nitrogen-rich porous carbon materials. The importance of the nitrogen content for the specific capacitance could be clearly seen from Figures 7a and 9 for NPC700 and NPC900, and it has been demonstrated previously.[48,49] NPC700 exhibited a better performance than NPC900, although the surface area and pore volume of NPC700 were smaller than that of NPC900 (Table 1). However, because both the pore geometry and nitrogen content contributes to the electrochemical properties,[18] the best performance was obtained for NPC800. To investigate the reusability, 1500 cycles of charge and discharge (Figure 10) were conducted successively on NPC800 at a current density of 3 A g^{-1}. Very little change in the specific capacitance was

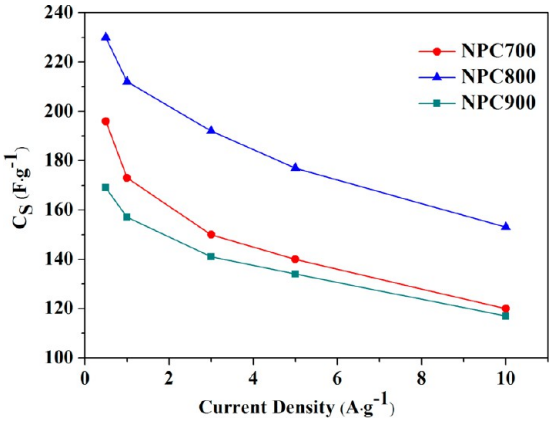

Figure 9. Relationship of the specific capacitance with respect to the charge−discharge current densities of NPC700, NPC800, and NPC900.

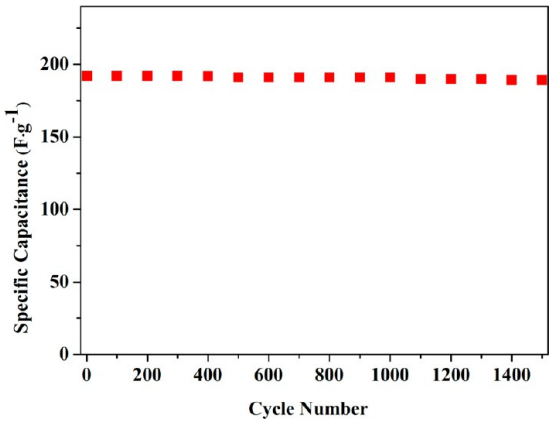

Figure 10. Cycling performance of the NPC800.

observed through the whole experiment, and 98% of the original capacitance was preserved after 1500 cycles.

4. CONCLUSIONS

In the present work, a POF was utilized to prepare nitrogen-rich porous carbon with a hollow, spherical structure by carbonization at high temperatures under a N_2 atmosphere. The prepared porous carbon exhibited better performance than the modified porous graphene reported previously.[50−52] The product carbonized at 800 °C showed a specific capacitance of 230 F g^{-1} at a current density of 0.5 A g^{-1} as well as good reusability. The presence of the nitrogen atoms and the hollow structure were responsible for the excellent supercapacitive performance. In comparison with the synthesis methods reported previously, the proposed method avoids the tedious preparation process. In addition, the micropore structure, the meso-morphology, and the nitrogen (or other heteroatoms) content of the final products can be tailored by the proper selection of precursor POFs and the carbonization process. Because the synthesis of various POFs is still undergoing rapid development, there are a very wide range of candidates for POF precursors with different structures and compositions for heteroatom-doped carbon frameworks that are suitable for use in supercapacitors. As mentioned previously, a specific capacitance as high as 304 F g^{-1} could be obtained with MPNCs, and it is reasonable to expect higher values for a more proper combination of carbon structures and dopants. However, porous carbon materials might have broad applications other than superconductors. Porous carbon with unique structures, various doping elements, and high specific surface areas might be of significance in molecule separation, catalysis, and drug delivery. The protocol utilized in the present work is therefore not limited to only an application in supercapacitors.

■ ASSOCIATED CONTENT

Supporting Information

Cyclic voltammograms of precursor POF, XRD data for NPC800, and nitrogen adsorption−desorption isotherms and pore size distribution data for NPC700 and NPC900. This material is available free of charge via the Internet at http://pubs.acs.org.

■ AUTHOR INFORMATION

Corresponding Author

*Tel: +86-931-8913813. Fax: +86-931-8912582. E-mail: puqs@lzu.edu.cn.

Notes

The authors declare no competing financial interest.

■ ACKNOWLEDGMENTS

The authors are grateful to the financial support of the National Natural Science Foundation of China (nos. 21175062, 21105040, and J1103307), the Specialized Research Fund for the Doctoral Program of Higher Education (20110211120010), and the Program for New Century Excellent Talents in University (NCET-08-0255) from the Ministry of Education, China.

■ REFERENCES

(1) Miller, J. R.; Simon, P. *Science* **2008**, *321*, 651−652.
(2) Frackowiak, E. *Phys. Chem. Chem. Phys.* **2007**, *9*, 1774−1785.
(3) Yu, G.; Hu, L.; Vosgueritchian, M.; Wang, H.; Xie, X.; McDonough, J. R.; Cui, X.; Cui, Y.; Bao, Z. *Nano Lett.* **2011**, *11*, 2905−2911.
(4) Wang, G.; Zhang, L.; Zhang, J. *Chem. Soc. Rev.* **2012**, *41*, 797−828.
(5) Pandolfo, A. G.; Hollenkamp, A. F. *J. Power Sources* **2006**, *157*, 11−27.
(6) Chen, W.; Rakhi, R. B.; Hu, L.; Xie, X.; Cui, Y.; Alshareef, H. N. *Nano Lett.* **2011**, *11*, 5165−5172.
(7) Winter, M.; Brodd, R. J. *Chem. Rev.* **2004**, *104*, 4245−4270.
(8) Chaikittisilp, W.; Ariga, K.; Yamauchi, Y. *J. Mater. Chem. A* **2013**, *1*, 14−19.
(9) Chaikittisilp, W.; Hu, M.; Wang, H.; Huang, H.-S.; Fujita, T.; Wu, K. C. W.; Chen, L.-C.; Yamauchi, Y.; Ariga, K. *Chem. Commun.* **2012**, *48*, 7259−7261.
(10) Liu, B.; Shioyama, H.; Akita, T.; Xu, Q. *J. Am. Chem. Soc.* **2008**, *130*, 5390−5391.
(11) Hall, P. J.; Mirzaeian, M.; Fletcher, S. I.; Sillars, F. B.; Rennie, A. J. R.; Shitta-Bey, G. O.; Wilson, G.; Cruden, A.; Carter, R. *Energy Environ. Sci.* **2010**, *3*, 1238−1251.
(12) Ma, F.; Zhao, H.; Sun, L.; Li, Q.; Huo, L.; Xia, T.; Gao, S.; Pang, G.; Shi, Z.; Feng, S. *J. Mater. Chem.* **2012**, *22*, 13464−13468.
(13) Qu, D.; Shi, H. *J. Power Sources* **1998**, *74*, 99−107.
(14) Zhang, H.; Cao, G.; Wang, Z.; Yang, Y.; Shi, Z.; Gu, Z. *Nano Lett.* **2008**, *8*, 2664−2668.
(15) Zhang, L. L.; Zhou, R.; Zhao, X. S. *J. Mater. Chem.* **2010**, *20*, 5983−5992.
(16) Zhang, L. L.; Zhao, X. S. *Chem. Soc. Rev.* **2009**, *38*, 2520−2531.
(17) Li, W.; Chen, D.; Li, Z.; Shi, Y.; Wan, Y.; Huang, J.; Yang, J.; Zhao, D.; Jiang, Z. *Electrochem. Commun.* **2007**, *9*, 569−573.

(18) Hulicova-Jurcakova, D.; Seredych, M.; Lu, G. Q.; Bandosz, T. J. *Adv. Funct. Mater.* **2009**, *19*, 438−447.
(19) Zhao, L.; Fan, L.-Z.; Zhou, M.-Q.; Guan, H.; Qiao, S.; Antonietti, M.; Titirici, M.-M. *Adv. Mater.* **2010**, *22*, 5202−5206.
(20) Hu, M.; Reboul, J.; Furukawa, S.; Radhakrishnan, L.; Zhang, Y.; Srinivasu, P.; Iwai, H.; Wang, H.; Nemoto, Y.; Suzuki, N.; Kitagawa, S.; Yamauchi, Y. *Chem. Commun.* **2011**, *47*, 8124−8126.
(21) Radhakrishnan, L.; Reboul, J.; Furukawa, S.; Srinivasu, P.; Kitagawa, S.; Yamauchi, Y. *Chem. Mater.* **2011**, *23*, 1225−1231.
(22) Chen, L.-F.; Zhang, X.-D.; Liang, H.-W.; Kong, M.; Guan, Q.-F.; Chen, P.; Wu, Z.-Y.; Yu, S.-H. *ACS Nano* **2012**, *6*, 7092−7102.
(23) Perego, C.; Millini, R. *Chem. Soc. Rev.* **2013**, *42*, 3956−3976.
(24) Ding, S.-Y.; Gao, J.; Wang, Q.; Zhang, Y.; Song, W.-G.; Su, C.-Y.; Wang, W. *J. Am. Chem. Soc.* **2011**, *133*, 19816−19822.
(25) Hu, M.; Reboul, J.; Furukawa, S.; Torad, N. L.; Ji, Q.; Srinivasu, P.; Ariga, K.; Kitagawa, S.; Yamauchi, Y. *J. Am. Chem. Soc.* **2012**, *134*, 2864−2867.
(26) Torad, N. L.; Hu, M.; Kamachi, Y.; Takai, K.; Imura, M.; Naito, M.; Yamauchi, Y. *Chem. Commun.* **2013**, *49*, 2521−2523.
(27) Pandey, P.; Katsoulidis, A. P.; Eryazici, I.; Wu, Y.; Kanatzidis, M. G.; Nguyen, S. T. *Chem. Mater.* **2010**, *22*, 4974−4979.
(28) Zhu, X.; Tian, C.; Mahurin, S. M.; Chai, S.-H.; Wang, C.; Brown, S.; Veith, G. M.; Luo, H.; Liu, H.; Dai, S. *J. Am. Chem. Soc.* **2012**, *134*, 10478−10484.
(29) Yang, G.; Han, H.; Du, C.; Luo, Z.; Wang, Y. *Polymer* **2010**, *51*, 6193−6202.
(30) Ariga, K.; Vinu, A.; Yamauchi, Y.; Ji, Q.; Hill, J. P. *Bull. Chem. Soc. Jpn.* **2012**, *85*, 1−32.
(31) Germain, J.; Svec, F.; Fréchet, J. M. J. *Chem. Mater.* **2008**, *20*, 7069−7076.
(32) Germain, J.; Frechet, J. M. J.; Svec, F. *J. Mater. Chem.* **2007**, *17*, 4989−4997.
(33) McKeown, N. B.; Budd, P. M. *Chem. Soc. Rev.* **2006**, *35*, 675−683.
(34) Mackintosh, H. J.; Budd, P. M.; McKeown, N. B. *J. Mater. Chem.* **2008**, *18*, 573−578.
(35) Jiang, J.-X.; Su, F.; Trewin, A.; Wood, C. D.; Niu, H.; Jones, J. T. A.; Khimyak, Y. Z.; Cooper, A. I. *J. Am. Chem. Soc.* **2008**, *130*, 7710−7720.
(36) Weber, J.; Thomas, A. *J. Am. Chem. Soc.* **2008**, *130*, 6334−6335.
(37) Han, S. S.; Furukawa, H.; Yaghi, O. M.; Goddard, W. A. *J. Am. Chem. Soc.* **2008**, *130*, 11580−11581.
(38) Ding, X.; Chen, L.; Honsho, Y.; Feng, X.; Saengsawang, O.; Guo, J.; Saeki, A.; Seki, S.; Irle, S.; Nagase, S.; Parasuk, V.; Jiang, D. *J. Am. Chem. Soc.* **2011**, *133*, 14510−14513.
(39) Kou, Y.; Xu, Y.; Guo, Z.; Jiang, D. *Angew. Chem., Int. Ed.* **2011**, *50*, 8753−8757.
(40) Feng, X.; Liang, Y.; Zhi, L.; Thomas, A.; Wu, D.; Lieberwirth, I.; Kolb, U.; Müllen, K. *Adv. Funct. Mater.* **2009**, *19*, 2125−2129.
(41) Liang, Y.; Feng, X.; Zhi, L.; Kolb, U.; Mullen, K. *Chem. Commun.* **2009**, 809−811.
(42) Yang, S.; Bachman, R. E.; Feng, X.; Müllen, K. *Acc. Chem. Res.* **2012**, *46*, 116−128.
(43) Friedel, B.; Greulich-Weber, S. *Small* **2006**, *2*, 859−863.
(44) Salyn, J. V.; Žumadilov, E. K.; Nefedov, V. I.; Scheibe, R.; Leonhardt, G.; Beyer, L.; Hoyer, E. *Z. Anorg. Allg. Chem.* **1977**, *432*, 275−279.
(45) Mishra, A. K.; Ramaprabhu, S. *Desalination* **2011**, *282*, 39−45.
(46) Li, W.; Zhang, F.; Dou, Y.; Wu, Z.; Liu, H.; Qian, X.; Gu, D.; Xia, Y.; Tu, B.; Zhao, D. *Adv. Energy Mater.* **2011**, *1*, 382−386.
(47) Garcia, B. B.; Candelaria, S. L.; Liu, D.; Sepheri, S.; Cruz, J. A.; Cao, G. *Renewable Energy* **2011**, *36*, 1788−1794.
(48) Hulicova, D.; Yamashita, J.; Soneda, Y.; Hatori, H.; Kodama, M. *Chem. Mater.* **2005**, *17*, 1241−1247.
(49) Kodama, M.; Yamashita, J.; Soneda, Y.; Hatori, H.; Kamegawa, K. *Carbon* **2007**, *45*, 1105−1107.
(50) Wang, Y.; Shi, Z.; Huang, Y.; Ma, Y.; Wang, C.; Chen, M.; Chen, Y. *J. Phys. Chem. C.* **2009**, *113*, 13103−13107.
(51) Wang, Y.; Guo, C. X.; Liu, J.; Chen, T.; Yang, H.; Li, C. M. *Dalton Trans.* **2011**, *40*, 6388−6391.
(52) Zhang, J.; Jiang, J.; Zhao, X. S. *J. Phys. Chem. C.* **2011**, *115*, 6448−6454.